

A Robust Framework for DOA Estimation: the Re-Iterative Super-Resolution (RISR) Algorithm

Shannon D. Blunt, *Senior Member, IEEE*, Tszping Chan, *Member, IEEE*,
and Karl Gerlach, *Fellow, IEEE*

This work was supported by the United States Office of Naval Research (ONR 31) and the Radar Division of the US Naval Research Lab and was presented in part at SAM 2008 - The Fifth IEEE Sensor Array & Multichannel Processing Workshop.

S.D. Blunt is with the Electrical Engineering & Computer Science Dept., Radar Systems & Remote Sensing Lab, of the University of Kansas, Lawrence, KS.

T. Chan was with the University of Kansas and is now with the Electrical & Computer Engineering Dept. at Johns Hopkins University, Baltimore, MD.

K. Gerlach is with the Radar Division of the US Naval Research Laboratory, Washington, DC.

Abstract

A new approach for spatial direction-of-arrival (DOA) estimation, denoted as Re-Iterative Super-Resolution (RISR), is developed based upon a recursive implementation of the minimum mean-square error (MMSE) framework. This recursive strategy alternates between updating an MMSE filter bank according to the previous receive spatial power distribution and then subsequently applying the new filter bank to the received data snapshots to obtain a new estimate of the receive spatial power distribution. Benefits of this approach include robustness to coherent sources such as can occur in multipath environments, operation with very low sample support to enable “tracking” of sources with rapidly changing DOA (*e.g.* bistatic pulse chasing), intrinsic determination of model order, and robustness to array modeling errors by exploiting approximate knowledge of array calibration tolerances. From an implementation perspective RISR belongs to a class of recursive algorithms that includes Interior Point methods, the minimum-norm based FoCal Underdetermined System Solver (FOCUSS) algorithm, and the Iterative Re-weighted Least Squares (IRLS) algorithm. However, the structure of RISR also enables the natural inclusion of spatial noise covariance information as well as a mechanism to account for array modeling errors which are known to induce degradation for existing super-resolution methods. The inclusion of the latter is also found to facilitate an adaptive form of regularization that establishes a feasible (given model uncertainties) dynamic range for source estimates.

Keywords

Beamforming, super-resolution, DOA estimation, MUSIC, ESPRIT, spatial smoothing,

MMSE, model order estimation, coherent sources, array modeling errors

I. INTRODUCTION

High resolution direction-of-arrival (DOA) estimation is the process of determining the individual spatial arrival angles (relative to some reference) of the collection of signals concurrently incident upon an antenna array (see [1–4] and references therein). Major applications in which DOA estimation is employed include radar, sonar, and wireless communications. The general problem formulation involves a collection of antenna elements upon which the superposition of a set of received signals is incident. At a given time instant, the sampled signal from each of the collection of antenna elements forms a spatial snapshot which is to be employed (possibly with other spatial snapshots) to determine the spatial DOA of each of the set of incident signals. However, some of these incident signals may arrive with a spatial separation that is too small to enable individual identification by means of the nominal array resolution. To identify sources spaced too closely for the nominal array resolution, numerous methods ([4] and references therein) have been developed in an effort to effectively deconstruct the superposition of incident signals into its individual components.

Two of the most well-known methods for DOA estimation are MUSIC [5–6] and ESPRIT [7], both of which employ the eigen-decomposition of a sample covariance matrix (SCM) formed from a collection of spatial snapshots. MUSIC exploits the orthogonality between a presumed “noise” subspace and a “signal” subspace. If the number of sources is known or estimated *a priori* (and is less than the number of antenna elements) and if the sources are temporally uncorrelated, then the angle estimation accuracy of MUSIC has been shown to converge asymptotically to the Cramer-Rao bound as the number of independent snapshots increases [6]. For linear arrays, the performance of MUSIC may be enhanced by using forward-backward averaging [8] and rooting techniques [9] (thus denoted as root-MUSIC). ESPRIT [7]

is based on a rotational invariance property of linear arrays and also employs the eigen-decomposition of a spatial SCM; thus performance is likewise enhanced by using forward-backward averaging. Similar performance has been observed for root-MUSIC and ESPRIT.

When the number of available snapshots is relatively small, such as may occur due to non-stationarity when the DOA of some sources change rapidly with time (*e.g.* due to rapid variations of the propagation medium and/or antenna motion, or when performing bistatic radar “pulse chasing” [10]) some degradation is observed for these SCM-based methods (relative to the case when the sample support is high) because of reduced estimation accuracy of the spatial covariance matrix. A more severe detriment to performance is the occurrence of spatially separated sources that possess temporal correlation [11–12], such as may result in multipath environments. It is also well-known that these techniques tend to be rather sensitive to array modeling errors [13–16].

The effects of temporal correlation may be remediated by spatial smoothing [11–12] whereby a smaller spatial covariance matrix is formed from overlapping sub-arrays. Of course, by employing spatial smoothing to estimate the SCM, fewer sources can be estimated due to the reduction in dimensionality. Also, even with spatial smoothing to ameliorate the temporal correlation effects, SCM-based techniques are still sensitive to array modeling errors which negatively impact both DOA estimation performance and model order selection performance.

A common link among previous approaches such as MUSIC and ESPRIT is the requirement to estimate the unknown spatial covariance matrix via a sample covariance matrix, which is calculated using the collection of spatial snapshots incident upon the array, and subsequently exploit the eigenstructure of the SCM to identify the number and DOA of the individual sources. In contrast, the method developed in this paper requires neither a sample

covariance matrix nor eigen-decomposition. The Re-Iterative Super-Resolution (RISR) algorithm is based on a recursive structured implementation of Minimum Mean-Square Error (MMSE) estimation that automatically determines the number of sources (*i.e.* no prior knowledge of the number of sources is required), their respective DOAs, and their respective magnitudes. Given spatial covariance information regarding the noise (which is simply the noise power if spatially white) and approximate knowledge of the array calibration tolerance (in terms of gain and phase), RISR operates by alternating between using the previous spatial power distribution to update the estimate of a structured MMSE filter bank and subsequently applying the filter bank to update the estimate of the spatial power distribution. From an implementation perspective RISR is related to a class of “recursively re-scaled” algorithms that include Interior Point methods [17–18] and the Minimum-Norm/Least-Squares based FOCUSS [19] and IRLS [20] methods. The novelty of RISR lies in *a*) the natural inclusion of the noise information within the estimator by virtue of the MMSE framework, *b*) a mechanism for non-coherent combining of multiple snapshots, and *c*) a structure to account for array modeling errors given approximate knowledge of the calibration tolerance. It should be noted that the manner of MMSE estimation employed by RISR is unrelated to the standard “data covariance” approaches that are adaptively scaled versions of the Minimum Variance Distortionless Response (MVDR) beamformer (see [21] and [4, pp. 440-447]). In addition, the RISR methodology is also directly applicable to high-resolution frequency estimation.

The remainder of the paper is organized as follows. Section II formulates the received signal model that is employed in Section III to derive the basic RISR structure. In Section IV this basic structure is generalized to accommodate multiple spatial snapshots and in Section V a modification to contend with array modeling errors is developed. Section VI discusses the

implementation of RISR. Finally, Section VII presents simulation results of the performance of RISR for various parameterizations and also compares performance with MUSIC, root-MUSIC and ESPRIT for various scenarios.

II. RECEIVED SIGNAL MODEL

Like the MUSIC algorithm, the formulation of RISR is applicable to any known array manifold (the issue of manifold ambiguities [22–23] is not considered here). Because it is so common, and to facilitate comparison with some well-known techniques (namely root-MUSIC and ESPRIT), we shall assume that the antenna is a linear array comprised of N equally-spaced identical elements that are ideally calibrated (array calibration errors will be addressed in a later section). Consider K signals, originating from sources in the far-field and satisfying the narrowband assumption (*i.e.* the bandwidth – aperture time delay product is $\ll 1$), that are concurrently incident upon the array (with $K \leq N$). Following A/D conversion, at the ℓ^{th} time sample the superposition of these signals along with noise can be represented in vector notation as the $N \times 1$ vector

$$\mathbf{y}(\ell) = \sum_{k=1}^K \mathbf{r}_k(\ell) + \mathbf{v}(\ell) \quad (1)$$

where $\mathbf{v}(\ell)$ is an $N \times 1$ vector of additive noise (of unknown distribution) and $\mathbf{r}_k(\ell)$ is the k^{th} incident signal defined as

$$\mathbf{r}_k(\ell) = x_k(\ell) \cdot \left[1 \quad e^{j\psi_k} \quad \dots \quad e^{j(N-1)\psi_k} \right]^T = x_k(\ell) \mathbf{s}(\psi_k) \quad (2)$$

with $x_k(\ell)$ the associated complex amplitude and $\mathbf{s}(\psi_k)$ the spatial steering vector (via the presumed known array manifold) corresponding to phase angle ψ_k . Note that the phase angle ψ

is functionally dependent on the spatial angle θ relative to the array boresight and subsumes the physical wavelength λ of the incident planewave and the array element spacing d . With the assumptions of narrowband signals impinging on a uniform linear array in the far-field, we shall henceforth simply address DOA estimation in terms of phase angle ψ .

Based on the received signal $\mathbf{y}(\ell)$ we wish to determine the direction-of-arrival (DOA) in ψ -space for each of the K incident signals at the ℓ^{th} time sample. This determination is accomplished by approximating the received signal model $\mathbf{y}(\ell)$ with a parameterized version as

$$\mathbf{y}(\ell) \cong \tilde{\mathbf{y}}(\ell) \triangleq \mathbf{S} \mathbf{x}(\ell) + \mathbf{v}(\ell). \quad (3)$$

The $N \times M$ matrix \mathbf{S} , generally with $M \gg N$, is obtained from the array manifold and defined as

$$\begin{aligned} \mathbf{S} &= [\mathbf{s}(0) \ \mathbf{s}(\psi_\Delta) \ \cdots \ \mathbf{s}((M-1)\psi_\Delta)] \\ &= \begin{bmatrix} 1 & 1 & \cdots & 1 \\ 1 & e^{j\psi_\Delta} & \cdots & e^{j(M-1)\psi_\Delta} \\ \vdots & \vdots & \cdots & \vdots \\ 1 & e^{j\psi_\Delta(N-1)} & \cdots & e^{j(M-1)\psi_\Delta(N-1)} \end{bmatrix}, \end{aligned} \quad (4)$$

being comprised of steering vectors with equally-spaced phase angles specified over 2π at an angular increment of $\psi_\Delta = \frac{2\pi}{M}$ (in effect, quantizing the phase angle ψ into M discrete values).

Note that larger values of M produce finer angular quantization, which in turn enable greater super-resolution capability (to the degree possible given noise, source correlation effects, and array modeling errors). The $M \times 1$ vector $\mathbf{x}(\ell)$ from (3) therefore contains a complex amplitude value associated with each of the M steering vectors in \mathbf{S} . Given sufficiently fine quantization of ψ , a comparison of (1) and (3) indicates that the $M \times 1$ vector $\mathbf{x}(\ell)$ would consist of all zeros

except for K non-zero values corresponding to the K sources. Thus the problem of DOA estimation is reformulated as the estimation of the parameterized vector $\mathbf{x}(\ell)$ from which the locations of the peaks (in ψ -space) are determined. Also, note that by estimating $\mathbf{x}(\ell)$, the source signal amplitudes are obtained as a direct result (unlike MUSIC or ESPRIT where the signal powers must be estimated afterwards). In like manner, the number of peaks in $\mathbf{x}(\ell)$ provides an estimate of model order.

A rather coarse estimate of $\mathbf{x}(\ell)$ can be obtained by employing a matched filter bank strategy in which the steering vector matrix \mathbf{S} is applied as

$$\begin{aligned}\hat{\mathbf{x}}_{\text{MF}}(\ell) &= \mathbf{S}^H \mathbf{y}(\ell) \\ &= \mathbf{S}^H \mathbf{S} \mathbf{x}(\ell) + \mathbf{S}^H \mathbf{v}(\ell)\end{aligned}\tag{5}$$

where $\{\bullet\}^H$ is the complex-conjugate transpose, or Hermitian, operation. The matched filter bank is also denoted as the *conventional beamformer* [3–4] as it is effectively an over-specified version of a Discrete Fourier Transform (DFT). It is this matched filter bank estimate that shall be employed as initialization for the recursive RISR algorithm.

III. RE-ITERATIVE SUPER-RESOLUTION

The RISR algorithm is based on the Minimum Mean-Square Error (MMSE) formulation and is motivated by the performance gains recently observed for an adaptive implementation of radar pulse compression originally denoted as Reiterative MMSE [24]. Using the received signal model defined in (3), RISR determines the $N \times M$ adaptive filter bank $\mathbf{W}(\ell)$ that minimizes the MMSE cost function

$$J = E \left\{ \left\| \mathbf{x}(\ell) - \mathbf{W}^H(\ell) \mathbf{y}(\ell) \right\|^2 \right\}. \quad (6)$$

Minimization of (6) yields the well-known MMSE filter structure

$$\mathbf{W}(\ell) = \left(E \left\{ \mathbf{y}(\ell) \mathbf{y}^H(\ell) \right\} \right)^{-1} E \left\{ \mathbf{y}(\ell) \mathbf{x}^H(\ell) \right\}. \quad (7)$$

Approximating $\mathbf{y}(\ell)$ with $\tilde{\mathbf{y}}(\ell)$, we substitute equation (3) into (7). Assuming the signal and noise components are statistically independent then results in

$$\mathbf{W}(\ell) = \left(\mathbf{S} E \left\{ \mathbf{x}(\ell) \mathbf{x}^H(\ell) \right\} \mathbf{S}^H + E \left\{ \mathbf{v}(\ell) \mathbf{v}^H(\ell) \right\} \right)^{-1} \mathbf{S} E \left\{ \mathbf{x}(\ell) \mathbf{x}^H(\ell) \right\}. \quad (8)$$

From (8), the noise covariance matrix is defined as $\mathbf{R} = E \left\{ \mathbf{v}(\ell) \mathbf{v}^H(\ell) \right\}$ which simplifies to

$\mathbf{R} = \sigma_v^2 \mathbf{I}$, with σ_v^2 the noise power, if spatially white. For the signal correlation term

$\mathbf{S} E \left\{ \mathbf{x}(\ell) \mathbf{x}^H(\ell) \right\} \mathbf{S}^H$ we make the simplifying assumption that the individual components of $\mathbf{x}(\ell)$

are temporally uncorrelated. This assumption is justified by the fact that the temporal

correlation, if any, between individual components of $\mathbf{x}(\ell)$ is generally unknown *a priori*. In

addition, noting that temporal correlation is a measure of statistical similarity over time, the

RISR formulation essentially operates on each snapshot independently (or at best combines

power estimates via non-coherent integration) and thus the temporal correlation of sources has

no meaning as far as the algorithm is concerned. Note that, while RISR is tolerant to source

correlation, some performance degradation is still observed as the coherent source scenario can

be likened to a severe reduction in sample support. To enforce the assumption of no temporal

correlation, we shall define the spatial power distribution matrix as

$$\mathbf{P}(\ell) = E \left\{ \mathbf{x}(\ell) \mathbf{x}^H(\ell) \right\} \odot \mathbf{I}_{M \times M} \quad (9)$$

where \odot is the Hadamard product and $\mathbf{I}_{M \times M}$ is an $M \times M$ identity matrix (to enforce the assumption that the sources are temporally uncorrelated), with the diagonal elements of $\mathbf{P}(\ell)$ comprising the spatial power distribution.

Substituting the noise covariance matrix and spatial power distribution matrix of (9) into (8) yields

$$\mathbf{W}(\ell) = \left(\mathbf{S} \mathbf{P}(\ell) \mathbf{S}^H + \mathbf{R} \right)^{-1} \mathbf{S} \mathbf{P}(\ell). \quad (10)$$

Of course, prior knowledge of $\mathbf{P}(\ell)$ is generally not available, hence the need to reiterate upon a previous estimate. Denoting the initial estimate of $\mathbf{x}(\ell)$ from (5) as $\hat{\mathbf{x}}_0(\ell) = \hat{\mathbf{x}}_{\text{MF}}(\ell)$, an initial estimate of the spatial power distribution is therefore

$$\hat{\mathbf{P}}_0(\ell) = \left[\hat{\mathbf{x}}_0(\ell) \hat{\mathbf{x}}_0^H(\ell) \right] \odot \mathbf{I}_{M \times M}. \quad (11)$$

In general, the previous estimate $\hat{\mathbf{P}}_{i-1}(\ell)$ is used to determine the new MMSE filter bank estimate $\hat{\mathbf{W}}_i(\ell)$ as

$$\hat{\mathbf{W}}_i(\ell) = \left(\mathbf{S} \hat{\mathbf{P}}_{i-1}(\ell) \mathbf{S}^H + \mathbf{R} \right)^{-1} \mathbf{S} \hat{\mathbf{P}}_{i-1}(\ell) \quad (12)$$

which is subsequently employed to obtain a new MMSE estimate of $\mathbf{x}(\ell)$ as

$$\hat{\mathbf{x}}_i(\ell) = \hat{\mathbf{W}}_i^H(\ell) \mathbf{y}(\ell). \quad (13)$$

In the same manner as (11), the i^{th} spatial power distribution estimate is computed as

$$\hat{\mathbf{P}}_i(\ell) = \left[\hat{\mathbf{x}}_i(\ell) \hat{\mathbf{x}}_i^H(\ell) \right] \odot \mathbf{I}_{M \times M}. \quad (14)$$

Equations (12), (13), and (14) comprise the i^{th} recursive stage of the basic form of RISR. The recursion may be halted when $\|\hat{\mathbf{x}}_i(\ell) - \hat{\mathbf{x}}_{i-1}(\ell)\|^2 < \varepsilon$ for ε some pre-determined small value or after some pre-determined number of stages. It has been observed anecdotally for linear arrays that RISR appears to always reach steady-state within 15 iterations regardless of the number of sources or the parameterization of the array and/or RISR. After the final iteration, the diagonal elements of the diagonal matrix $\sqrt{\mathbf{P}_i(\ell)}$ are the ‘‘RISR spectrum’’ and provide an estimate of the spatial magnitude distribution corresponding to the demarcation of ψ -space.

IV. NON-COHERENT INTEGRATION

As derived above, RISR can be applied to a single spatial snapshot. However, RISR may also be generalized to accommodate non-coherent integration of multiple time samples (assuming stationarity of the spatial power distribution over the given time interval). It will be shown that this generalization provides significant performance improvement for RISR. Note that this non-coherent integration procedure is applicable to any array geometry.

To employ non-coherent integration over L time samples, an aggregate filter bank $\bar{\mathbf{W}}$ is formed which is to be applied to a collection of L spatial receive snapshots $\mathbf{Y} = [\mathbf{y}(\ell) \ \mathbf{y}(\ell+1) \ \cdots \ \mathbf{y}(\ell+L-1)]$ as

$$\hat{\mathbf{X}} = \bar{\mathbf{W}}^H \mathbf{Y} \quad (15)$$

where $\hat{\mathbf{X}} = [\hat{\mathbf{x}}(\ell) \ \hat{\mathbf{x}}(\ell+1) \ \cdots \ \hat{\mathbf{x}}(\ell+L-1)]$ is a $M \times L$ matrix comprised of the spatial complex amplitude estimates for the L snapshots. An aggregate spatial power distribution estimate is then determined as

$$\bar{\mathbf{P}} = \left[\frac{1}{L} \sum_{\tau=0}^{L-1} \hat{\mathbf{x}}(\ell + \tau) \hat{\mathbf{x}}^H(\ell + \tau) \right] \odot \mathbf{I}_{M \times M}. \quad (16)$$

For the i^{th} recursion, the average power estimate $\bar{\mathbf{P}}_{i-1}$ replaces the estimate $\hat{\mathbf{P}}_{i-1}(\ell)$ in (12) to estimate the aggregate MMSE filter bank $\bar{\mathbf{W}}_i$. The matched filter bank initialization is performed as previously discussed with \mathbf{S} from (4) being applied to the set of L snapshots. Because it subsumes the single snapshot implementation (*i.e.* $L=1$), it shall henceforth be presumed that RISR employs non-coherent integration of L time samples.

V. ARRAY MODELING ERRORS

We now consider the effects of modeling errors that will always be present in practice due to antenna element location uncertainty, realistic calibration tolerances, mutual coupling effects between elements, etc. Quantization error due to finite precision sampling in amplitude and phase may likewise be grouped into this category. As with non-coherent integration, the following formulation is likewise applicable to any array geometry.

We shall attempt to make as few assumptions about the modeling errors as possible since, by definition, they are an unknown quantity. Specifically, for the sake of mathematical tractability, the following assumptions are made:

- 1) the distributions of amplitude and phase modeling errors are i.i.d. for each antenna element and are each zero-mean and symmetric (thus the modeling errors across elements are uncorrelated), and
- 2) the modeling errors, the source signals, and the additive noise are all statistically independent.

First, the array response accounting for possible modeling errors is defined as

$$\mathbf{y}_{err}(\ell) \triangleq (\mathbf{S}\mathbf{x}(\ell)) \odot \mathbf{z} + \mathbf{v}(\ell) \quad (17)$$

where \odot is the Hadamard product and the $N \times 1$ vector \mathbf{z} incorporates the (unknown) modeling errors. Note that (17) presupposes that the modeling errors are independent of source DOA. The n^{th} element of \mathbf{z} can be generically modeled as

$$z_n = [1 + \Delta_{a,n}] \exp\{j\Delta_{\phi,n}\} \quad (18)$$

where $\Delta_{a,n}$ is the random amplitude deviation of arbitrary distribution and $\Delta_{\phi,n}$ is the random phase deviation of arbitrary distribution. We define the element error variance of z_n from (18) as σ_z^2 (the same for all antenna elements based on assumption 1). To accommodate the modeling errors in the structure of RISR, we shall approximate them as an additional source of noise as

$$\mathbf{y}_{err}(\ell) = (\mathbf{S}\mathbf{x}(\ell)) \odot \mathbf{z} + \mathbf{v}(\ell) \approx \mathbf{S}\mathbf{x}(\ell) + \mathbf{v}(\ell) + \mathbf{v}_z(\ell) \quad (19)$$

where $\mathbf{v}_z(\ell) = (\mathbf{S}\mathbf{x}(\ell)) \odot (\mathbf{z} - \mathbf{1}_{N \times 1})$ is the “noise” induced by modeling errors. Note that according to assumption 1 and the generic model in (18), $\mathbf{v}_z(\ell)$ is likewise zero-mean.

Using assumptions 1 and 2, it is straightforward to show that in the presence of modeling errors the RISR filter bank estimate in (12) becomes

$$\hat{\mathbf{W}}_m(\ell) = \left(\mathbf{S} \hat{\mathbf{P}}_{m-1}(\ell) \mathbf{S}^H + \mathbf{R} + \mathbf{R}_z \right)^{-1} \mathbf{S} \hat{\mathbf{P}}_{m-1}(\ell) \quad (20)$$

where $\mathbf{R}_z = E\{\mathbf{v}_z(\ell) \mathbf{v}_z^H(\ell)\}$ is the “model noise” covariance matrix. Substituting in the presumed model noise from above yields

$$\begin{aligned}
\mathbf{R}_z &= E \left\{ \left(\mathbf{z} - \mathbf{1}_{N \times 1} \right) \odot \left(\mathbf{S} \mathbf{x}(\ell) \right) \left(\mathbf{S} \mathbf{x}(\ell) \right)^H \odot \left(\mathbf{z} - \mathbf{1}_{N \times 1} \right)^H \right\} \\
&= E \left\{ \tilde{\mathbf{Z}} \left(\mathbf{S} \mathbf{x}(\ell) \right) \left(\mathbf{S} \mathbf{x}(\ell) \right)^H \tilde{\mathbf{Z}}^H \right\}
\end{aligned} \tag{21}$$

where $\tilde{\mathbf{Z}} = \text{diag} \{ z_0, z_1, \dots, z_{N-1} \} - \mathbf{I}_{N \times N}$. Then using assumption 1 (uncorrelated modeling errors) and assumption 2 (source signal and modeling error independence), it can be shown that (21) simplifies to

$$\mathbf{R}_z = \sigma_z^2 \mathbf{I}_{N \times N} \odot \left(\mathbf{S} \mathbf{P}(\ell) \mathbf{S}^H \right). \tag{22}$$

Given that the presumed model noise covariance is dependent on the source spatial power distribution via (22), and taking into account non-coherent integration of multiple snapshots, the filter bank update is thus

$$\bar{\mathbf{W}}_i = \left(\mathbf{S} \bar{\mathbf{P}}_{i-1} \mathbf{S}^H + \sigma_z^2 \mathbf{I}_{N \times N} \odot \left(\mathbf{S} \bar{\mathbf{P}}_{i-1} \mathbf{S}^H \right) + \mathbf{R} \right)^{-1} \mathbf{S} \bar{\mathbf{P}}_{i-1}. \tag{23}$$

VI. IMPLEMENTATION

The application of equations (15), (16), and (23) in a recursive manner form the basis of the RISR algorithm. As was discussed in Section V the impact of array modeling error, which will always be present in practice, can be accounted for via the σ_z^2 term in (23). If the additive noise is spatially white, then the noise covariance term $\mathbf{R} = \sigma_v^2 \mathbf{I}$ and the model noise covariance term $\mathbf{R}_z = \sigma_z^2 \mathbf{I}_{N \times N} \odot \left(\mathbf{S} \mathbf{P}(\ell) \mathbf{S}^H \right)$ can both be viewed as regularization (or diagonal loading) terms. Specifically, the noise covariance term $\mathbf{R} = \sigma_v^2 \mathbf{I}$ is a (fixed) noise-dependent loading term and the model noise covariance term $\mathbf{R}_z = \sigma_z^2 \mathbf{I}_{N \times N} \odot \left(\mathbf{S} \mathbf{P}(\ell) \mathbf{S}^H \right)$ is a signal-dependent

loading term that is thus adaptive in nature according to the update of the source estimates. This latter term essentially serves to establish an “acceptable” dynamic range for the set of source estimates thereby eliminating spurious peaks that could otherwise arise due to array modeling errors or under-estimation of the noise power when high-power sources are present. In fact, this effect may be exploited by enabling a reduction in the noise covariance term $\mathbf{R} = \sigma_v^2 \mathbf{I}$. Reduction of this term alone has been found to improve the sensitivity of RISR albeit with the undesired side-effect of small spurious peaks for the high SNR regime. The presence of the model noise covariance term eliminates these spurious peaks thus facilitating enhanced sensitivity. Hence, (23) can be slightly modified as

$$\bar{\mathbf{W}}_i = \left(\mathbf{S} \bar{\mathbf{P}}_{i-1} \mathbf{S}^H + \sigma_z^2 \mathbf{I}_{N \times N} \odot \left(\mathbf{S} \bar{\mathbf{P}}_{i-1} \mathbf{S}^H \right) + \alpha \mathbf{R} \right)^{-1} \mathbf{S} \bar{\mathbf{P}}_{i-1}. \quad (24)$$

where the term $\alpha \mathbf{R}$, for $0 < \alpha \leq 1$, provides a scaled noise covariance term that is compensated for at high SNR values by the model noise covariance term (*i.e.* the adaptive regularization). For this reason (and given the fact that the case of zero array modeling error is purely theoretical), some nominal value of σ_z^2 is necessitated. It has been found for small/moderate size linear arrays ($N \leq 20$) that, in the theoretically idealistic case of no array modeling errors, values of σ_z^2 less than -30 dB tend to induce false peaks. Likewise, it has been found that the value of α should not be too small or else the intrinsic benefit of regularization via the noise covariance term, which is particularly important in low SNR scenarios, is sacrificed.

Given the final modification from (24), the complete operation of RISR is outlined in Table 1. It is found that for each iteration, the computational cost of RISR is $O(MNL)$ for $L > 2N$ and $O(MN^2)$ otherwise, where M is generally some multiple of N . Thus RISR is more computationally expensive than the SCM-based methods such as MUSIC which require

$O(LN^2)$ to compute the sample covariance matrix and $O(N^3)$ to compute the eigen-decomposition.

Table 1. Operation of RISR

<p>Initialization: Given L receive snapshots $\mathbf{Y} = [\mathbf{y}(\ell) \ \mathbf{y}(\ell+1) \ \dots \ \mathbf{y}(\ell+L-1)]$, compute initial complex amplitude distribution as $\hat{\mathbf{X}}_0 = \mathbf{S}^H \mathbf{Y}$. Compute the initial average spatial power distribution estimate as $\bar{\mathbf{P}}_0 = \left[\frac{1}{L} \sum_{\tau=0}^{L-1} \hat{\mathbf{x}}_0(\ell+\tau) \hat{\mathbf{x}}_0^H(\ell+\tau) \right] \odot \mathbf{I}_{M \times M}$. Determine the noise-only covariance matrix \mathbf{R} (or just the noise power if presumed to be spatially white) and select the noise loading factor α. Based on expected model error tolerances determine the model error variance σ_z^2.</p> <p>For $i = 1, 2, \dots$ until recursion halted</p> <ol style="list-style-type: none"> 1) Determine the aggregate MMSE filter bank as $\bar{\mathbf{W}}_i = \left(\mathbf{S} \bar{\mathbf{P}}_{i-1} \mathbf{S}^H + \sigma_z^2 \mathbf{I}_{N \times N} \odot \left(\mathbf{S} \bar{\mathbf{P}}_{i-1} \mathbf{S}^H \right) + \alpha \mathbf{R} \right)^{-1} \mathbf{S} \bar{\mathbf{P}}_{i-1}.$ 2) Estimate the spatial complex amplitude estimates for the L snapshots as $\hat{\mathbf{X}}_i = \bar{\mathbf{W}}_i^H \mathbf{Y}$. 3) Compute $\bar{\mathbf{P}}_i = \left[\frac{1}{L} \sum_{\tau=0}^{L-1} \hat{\mathbf{x}}_i(\ell+\tau) \hat{\mathbf{x}}_i^H(\ell+\tau) \right] \odot \mathbf{I}_{M \times M}$ to update the estimate of the spatial power distribution. <p>Once recursion is halted, obtain spatial magnitude distribution (<i>i.e.</i> the RISR spectrum) as $\bar{\mathbf{x}} = \text{diag} \left\{ \sqrt{\bar{\mathbf{P}}_i} \right\}$. Determine number of sources, source locations (in ψ-space), and source magnitude estimates via the peaks in $\bar{\mathbf{x}}$.</p>

VII. SIMULATION RESULTS

Using the implementation of (12), the performance of RISR was previously compared with MUSIC for cases involving equal-power sources [25]. Here we shall compare RISR (based on the implementation in Table 1) to MUSIC, root-MUSIC (denoted here as RMUSIC), and ESPRIT. For scenarios involving temporally correlated sources, spatially-smoothed (SS) implementations are employed (denoted as SS-MUSIC, SS-RMUSIC, and SS-ESPRIT). When estimating the spatial sample covariance matrix (SCM) for MUSIC, RMUSIC, and ESPRIT (as well as for the spatially smoothed implementations) forward-backward averaging is used. Note that it has been observed that no benefit is obtained for RISR when the “backward” snapshots are included as RISR does not require a spatial SCM.

Before comparing with other methods, we first consider the effects of various parameterizations on RISR in the hypothetical “error-free” scenario by varying the number of snapshots L , the amount of source separation angle, the number of antenna elements N (for the linear array structure), the amount of angular “over-sampling” (by varying the ratio M/N), and the factor α that scales the noise covariance term. An example of the convergence behavior of RISR is also presented. For all cases, stated values of SNR are the incident signal-to-noise ratio for a single antenna element.

Unless otherwise stated, we shall employ a linear array of $N=10$ elements with half-wavelength spacing. Assuming ideal half-wavelength element spacing, the $N=10$ element linear array provides a nominal resolution (in terms of electrical angle) of $(\Delta\psi)_{\text{nom}} = 2\pi/M = 36^\circ$. To examine super-resolution capability we consider the separation of two closely-spaced sources, both alone ($K=2$) and in the presence of other sources ($K \geq 3$). Defining array boresight as $\psi = 0^\circ$, two closely spaced sources are placed in the vicinity of 0°

with some fixed separation (dictated by the particular scenario). Note that the two sources near $\psi = 0^\circ$ can be used to convey performance in general due to the rotational invariance of ψ -space [4]. After the matched filter bank initialization, 15 recursions of RISR are performed. All Monte Carlo simulations employ 500 runs for each individual value (of SNR or percent modeling error).

The sources will be modeled as being constant-modulus random-phase signals experiencing i.i.d. random fading (independently assigned for each Monte Carlo run). The fading magnitude is Rayleigh distributed with a given source power level and the phase is uniformly distributed over 2π . The fading is constant over the interval of L snapshots. When coherent sources are considered, the K source directions all possess the same constant-modulus random-phase signal and experience independent fading. The additive noise is complex white Gaussian (note that RISR makes no assumption regarding the noise distribution other than it being zero-mean and the power is estimated with sufficient accuracy).

For the results presented here the SCM-based MUSIC, RMUSIC, and ESPRIT methods are applied with clairvoyant knowledge of the number of sources K . Thus RMUSIC and ESPRIT each provide K source estimates. The MUSIC source estimates are the K peaks that appear in the MUSIC pseudo-spectrum. For RISR the number of sources is unknown and must be determined by locating suitable peaks in the RISR spectrum $\bar{\mathbf{x}}$. For the results shown here a peak is decided if an element in the RISR spectrum is greater than the immediately surrounding elements and, because RISR provides an estimate of the spatial power distribution, a peak must also be greater than the normalized beamformer output noise power σ_v^2/N . The number of peaks detected by RISR constitutes the model order estimate. To assess model order estimation performance of RISR, it is compared with the Minimum Description Length metric [26] which

has been shown to be the most appropriate for the low sample support regime [27]. It will be shown that RISR model order estimate performance tends to track closely with separation probability performance.

Denoting the two closely-spaced sources as ψ_1 and ψ_2 , where $\psi_1 < \psi_2$, the two sources are deemed separated when exactly two sources are estimated to exist within an interval bounded between $-0.5(\Delta\psi)_{\text{nom}} + \psi_1$ and $+0.5(\Delta\psi)_{\text{nom}} + \psi_2$. For scenarios with more than two sources (*i.e.* $K \geq 3$), the phase angles of the additional sources are randomly distributed (with a uniform distribution for each Monte Carlo run) over 2π except for the $\pm(\Delta\psi)_{\text{nom}}$ interval centered on $\psi = 0^\circ$ so as to avoid association problems with the two closely-spaced sources. The separation probability is determined as the ratio of the number of times the two closely-spaced sources are successfully separated to the number of Monte Carlo runs (here this is 500). If the two sources are deemed separated, the estimated RMS error (or simply RMS error) for the two sources is then computed as

$$\text{RMS error} = \sqrt{\left[\frac{1}{K} \sum_{k=1}^K |\psi_k - \hat{\psi}_k|^2 \right]} \quad (25)$$

where ψ_k and $\hat{\psi}_k$ are the phase angles for the true DOA and estimated DOA, respectively, for the two closely-spaced sources. It should be noted when comparing RMS error that one must also consider the corresponding probability of separation so as to avoid misleading comparisons (*e.g.* too few detections of separated peaks for a given Monte Carlo run may yield an inaccurate estimate of RMS error due to insufficient data). To alleviate this potential confusion, RMS error results are only shown for Monte Carlo results achieving a separation probability $\geq 20\%$.

A. RISR PARAMETERIZATION ASSESSMENT

The performance of RISR is assessed as a function of 1) sample support size L , 2) the degree of separation of two closely-spaced sources, 3) the number of array elements N , 4) the angular over-sampling factor M/N , and 5) the noise covariance scaling factor α . For parameterization assessment the two sources are temporally uncorrelated and no array modeling errors are present. For this idealistic scenario a nominal value of element error variance parameter for the RISR algorithm will be set to $\sigma_z^2 = 3 \times 10^{-3} \approx -25$ dB.

Before considering the impact of parameterization let us first examine the convergence of RISR. For two sources near $\psi = -90^\circ$ with an SNR of 10 dB, $L = 12$ snapshots, an over-sampling factor of $M/N = 16$, a noise covariance scaling of $\alpha = 1$, and a separation of $1/4 (\Delta\psi)_{\text{nom}}$ (*i.e.* 9° for $N = 10$ antenna elements), Fig. 1 depicts the estimated spatial power distribution for the initial matched filter bank (the conventional beamformer) and for the application of RISR after 2, 4, 6, 8, and 10 iterations. It is observed that the spatial sidelobes have been essentially eliminated after 2 iterations and after 6 iterations the two sources are just beginning to resolve themselves. After 8 iterations the two sources are clearly resolved and after 10 iterations essentially the only non-zero values are those corresponding to the source estimate locations in ψ -space. Note that the source estimates have converged to the true source powers of unity (0 dB). For more complicated scenarios such as high source dynamic range (the ratio of the largest source power to the smallest source power) or when numerous sources are present it may take more iterations to converge. However, it has been observed anecdotally for linear arrays that this is almost always accomplished within 15 iterations regardless of the parameterization.

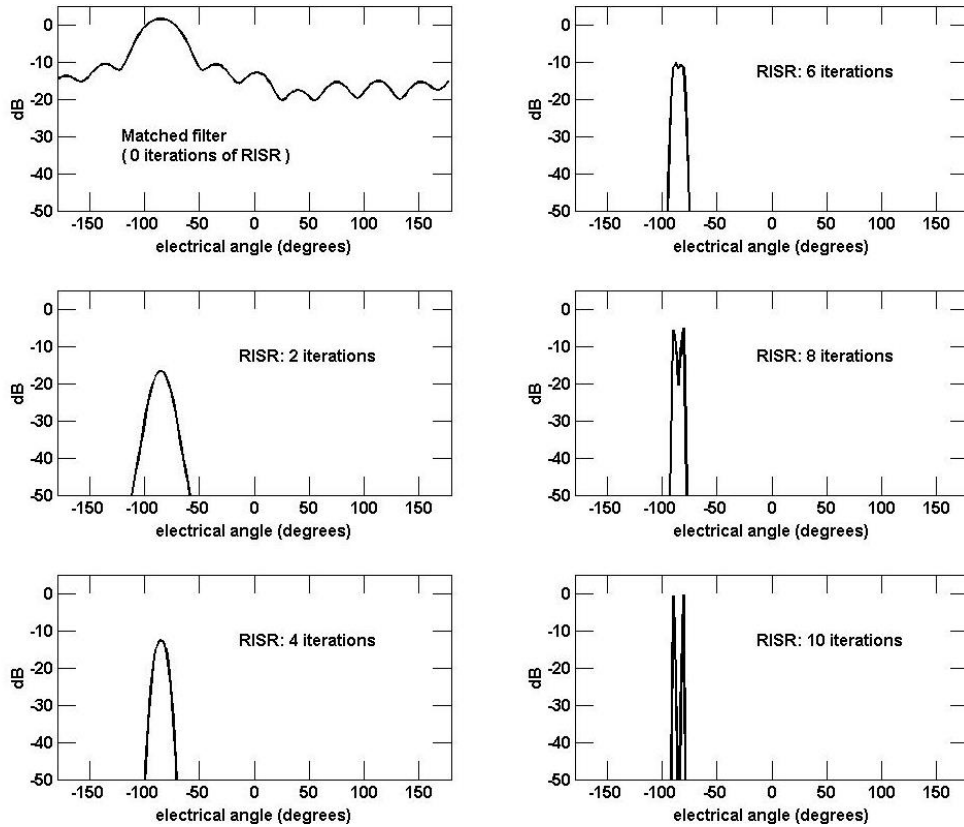


Figure 1. Convergence of RISR for $M/N = 16$, $N = 10$, $L = 12$, sources separated by $1/4$ nominal resolution, and $\text{SNR} = 10$ dB

For the sample support comparison, values of $L = 1, 2, 4, 8$, and 16 snapshots are examined. Figures 2 and 3 illustrate the performance of RISR for two sources with an oversampling factor of $M/N = 16$, a separation of $1/2 (\Delta\psi)_{\text{nom}}$ (*i.e.* 18° for $N = 10$ antenna elements), and $\alpha = 1/8$ (the appropriate selection of α will be addressed in subsequent discussion).

Figure 2 illustrates the probability of separation (top panel) and RMS error (bottom panel) of RISR as a function of SNR for the different numbers of snapshots. It is observed that as the number of snapshots increases, RISR requires a lower SNR in order to achieve the same separation probability (most notably at higher probability of separation). The improvement is

most dramatic when increasing from $L=1$ to $L=2$ with the improvement becoming more gradual thereafter. Improvement is likewise observed for RMS error which decreases by roughly half when increasing the number of snapshots from $L=1$ to $L=2$. The improvement in separation probability and RMS error becomes less pronounced as L increases further.

It is worth noting that the separation probability approaches, yet never quite reaches, a probability of 1. This effect is due to the fact that the sources experience (sometimes significant) fading yet RISR operates effectively only over a finite dynamic range due in part to the non-zero value of σ_z^2 . It is also observed that, above 20 dB SNR, the RMS error for $L=4, 8$ and 16 does not continue to decrease. This effect occurs because the “sampling” of ψ -space dictated by the $N \times M$ steering vector matrix \mathbf{S} establishes an angular quantization lower bound that is directly related to an “over-sampled resolution limit” of $2\pi/M$.

Figure 3 depicts the ability of RISR to determine the model order which is simply the number of peaks found in $\bar{\mathbf{x}}$. Figure 3 presents the mean order estimate (top panel) and the probability of correctly estimating the order (bottom panel) as a function of SNR. It is observed that increasing L has a distinct impact on the accuracy of the model order estimate. This improvement is the most pronounced for small L while little difference is observed when L is increased from 8 to 16. It is also noted that small L tends to result in an over-estimation of model order as opposed to under-estimation.

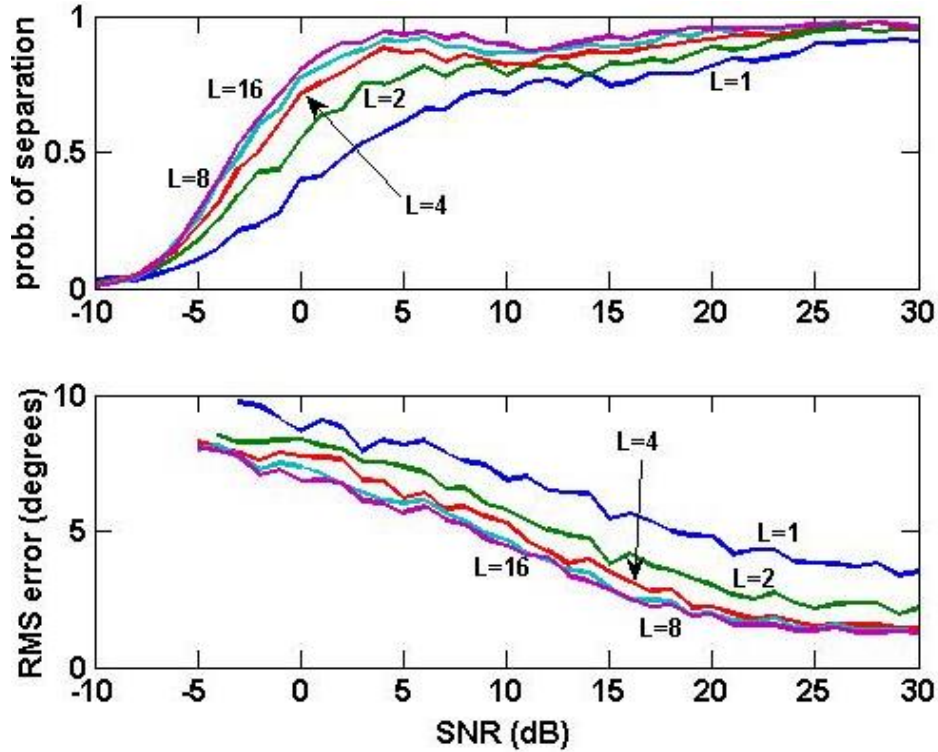


Figure 2. RISR: source separation performance vs. SNR for 2 sources (separation of 1/2 the nominal resolution) for various sample support, $M/N = 16$, $\alpha = 1/8$, and $N = 10$

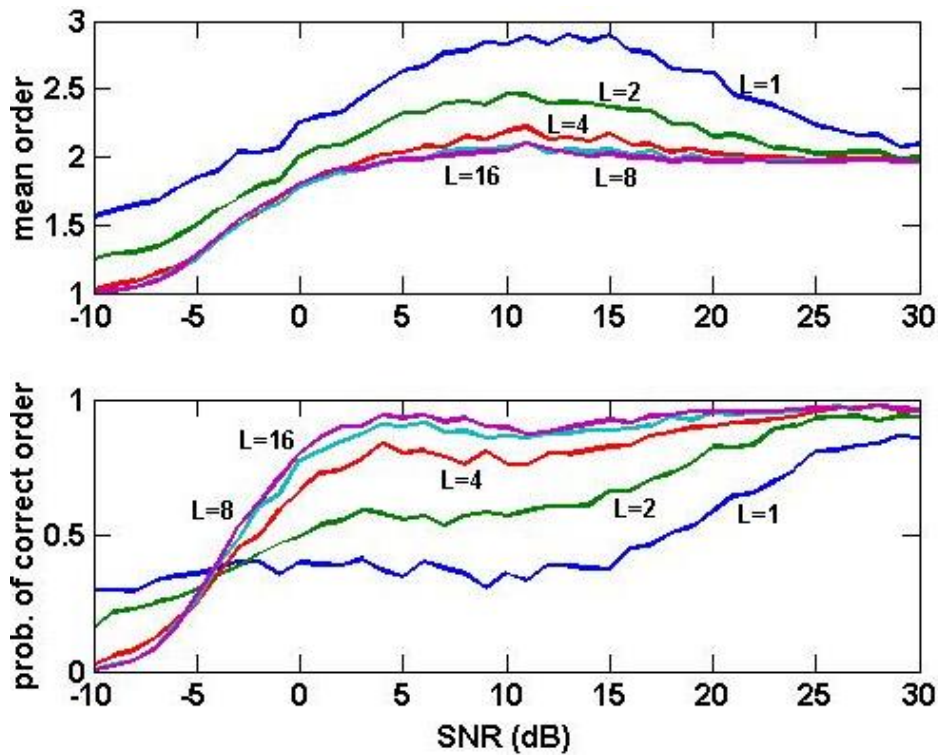


Figure 3. RISR: model order selection vs. SNR for 2 sources (separation of 1/2 the nominal resolution) for various sample support, $M/N = 16$, $\alpha = 1/8$, and $N = 10$

We now consider the effect of the amount of source separation on RISR performance. Three different scenarios are addressed, each with a different separation between the two sources. Specifically, with $N = 10$ yielding a nominal resolution of $(\Delta\theta)_{\text{nom}} = 36^\circ$, the three scenarios each contain two sources with separations of *a*) $1/2(\Delta\theta)_{\text{nom}} = 18^\circ$, *b*) $1/4(\Delta\theta)_{\text{nom}} = 9^\circ$, and *c*) $1/8(\Delta\theta)_{\text{nom}} = 4.5^\circ$.

Figure 4 illustrates the performance of RISR for these three scenarios when $L = 15$ snapshots are present, noise covariance scaling factor $\alpha = 1/8$, and a spatial over-sampling of $M/N = 16$. It is observed that the probability of separation (top panel) degrades slightly from the case of $1/2(\Delta\theta)_{\text{nom}}$ to $1/4(\Delta\theta)_{\text{nom}}$, with the degradation more pronounced when the source separation further decreases to $1/8(\Delta\theta)_{\text{nom}}$. Model order estimation performance (probability of correct order) is not shown as the results are essentially identical to that observed in the top panel of Fig. 4. In the bottom panel of Fig. 4 the RMS error is depicted. For low SNR values it is observed that smaller source separation yields lower RMS error. Referring to the convergence of RISR illustrated by Fig. 1 in which the single peak splits into two nearby peaks as the algorithm progresses, one may readily infer that angle estimate errors tend more towards under-estimating the amount of separation of nearby sources as opposed to over-estimation. As a result, smaller separation angles tend to yield lower RMS error.

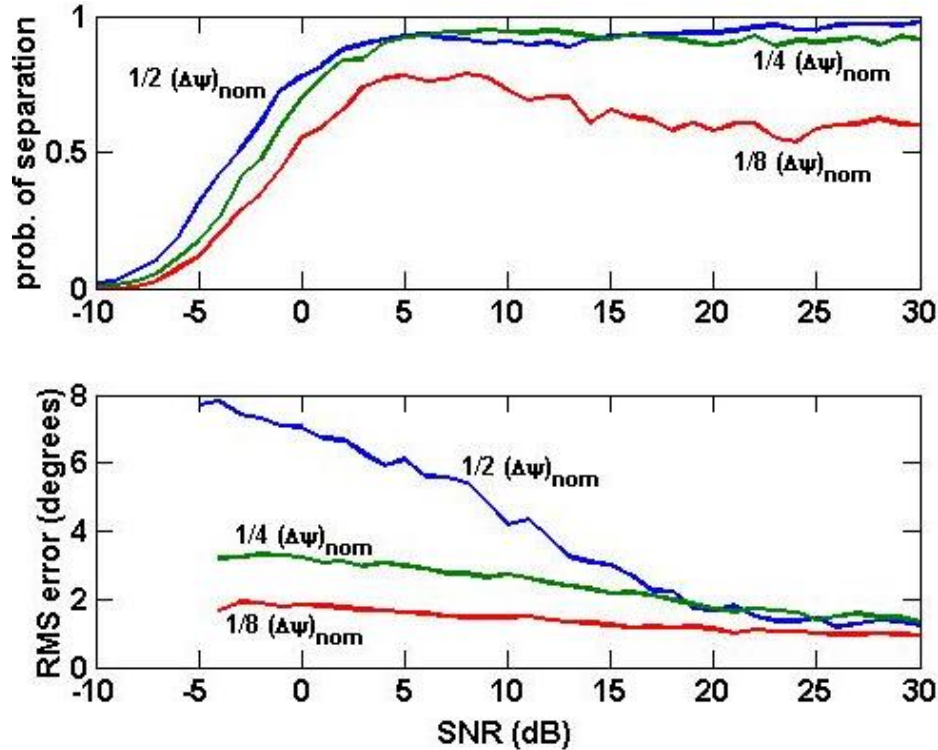


Figure 4. RISR: source separation performance vs. SNR as a function of the angular separation between 2 sources for $L=15$, $M/N=16$, $\alpha=1/8$, and $N=10$

We now examine the performance of RISR as a function of the number of antenna elements N . Specifically, we consider $N=5, 10, 20$, and 40 such that the nominal resolution $(\Delta\theta)_{\text{nom}}$ of each is $72^\circ, 36^\circ, 18^\circ$, and 9° , respectively. We consider 2 sources with separation of $1/2(\Delta\theta)_{\text{nom}}$ or $36^\circ, 18^\circ, 9^\circ$, and 4.5° , respectively, for each N . For $L=15$ snapshots, angular over-sampling of $M/N=16$, and noise covariance scaling $\alpha=1/8$, Fig. 5 illustrates the probability of separation (top panel) and RMS error (bottom panel) for the four different array sizes. Note that the model order estimation performance is again omitted because the curves were nearly identical to those for separation probability. It is evident from Fig. 5 that, as one would expect, the separation probability as a function of SNR shifts 3 dB to the left for each doubling of the array size. The RMS error is likewise halved for each doubling of the array size.

It is also observed that as N increases a slight dip becomes more pronounced. This effect is related to the particular choice of α which will be discussed subsequently.

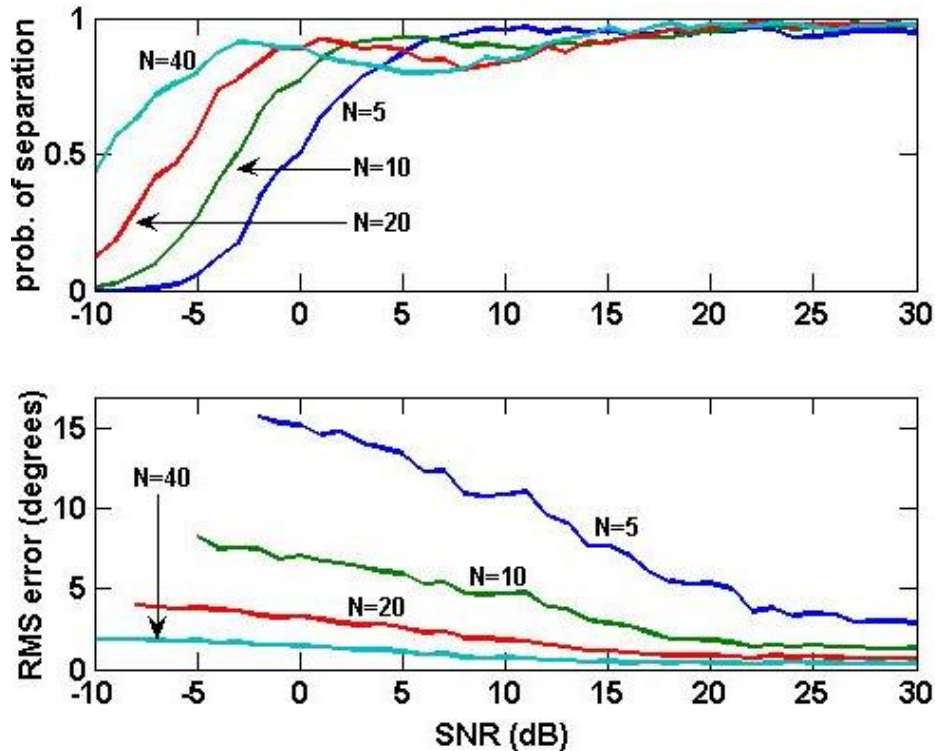


Figure 5. RISR: source separation performance vs. SNR for 2 sources at $1/2$ nominal resolution as a function of the number of array elements N for $L=15$, $M/N=16$, and $\alpha=1/8$

We consider the impact of the degree of over-sampling in ψ -space (*i.e.* the value of M/N) on the performance of RISR. For an $N=10$ element linear array, $L=15$ snapshots, noise covariance scaling $\alpha=1/8$, and two sources with separation $1/2(\Delta\theta)_{\text{nom}}=18^\circ$ (*i.e.* super-resolution factor of two), we consider values for M/N of 4, 8, 16, and 32. Thus the number of columns in the steering vector matrix \mathbf{S} is 40, 80, 160, and 320, respectively. Note that there is no restriction on M/N being a multiple of 2; it is done here simply for convenience. Figure 6 illustrates the performance of RISR for these four scenarios. Model order

estimation performance is again omitted because the curves are nearly identical to those for separation probability in Fig. 6. It is observed that as M/N increases higher SNR is needed to achieve a moderate separation probability (0.5 for example). However, for higher separation probability (above 0.9) a lower SNR is required for larger values of M/N .

In the bottom panel of Fig. 6 it is observed that the RMS error decreases as M/N decreases. Note also that as M/N increases an RMS error floor occurs at successively higher SNR values. This error floor is due to the finite quantization of ψ -space discussed previously.

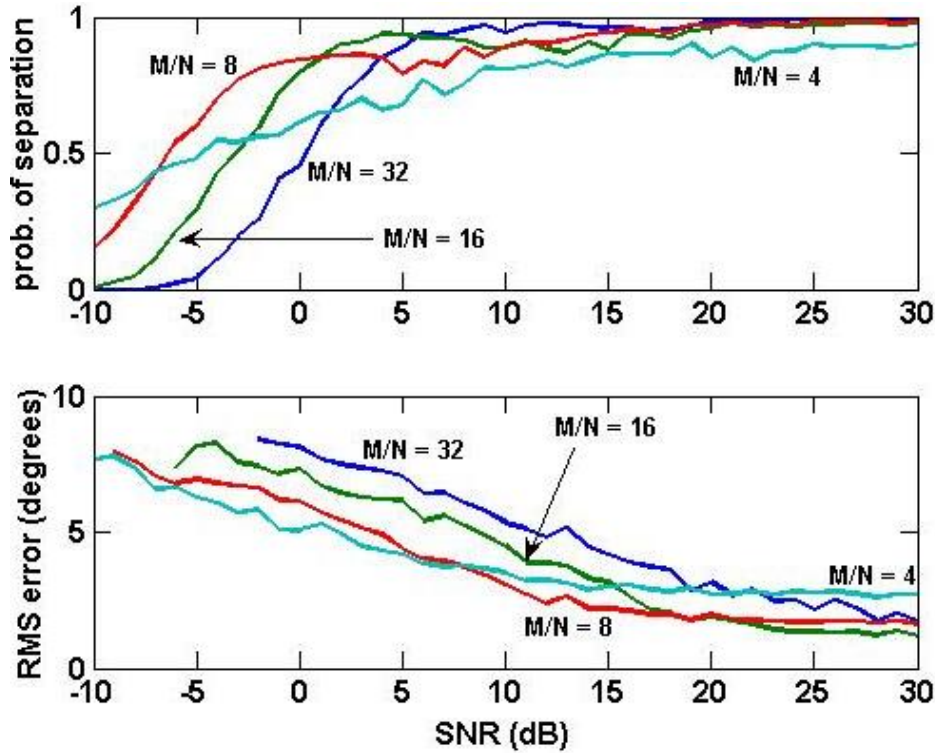


Figure 6. RISR: source separation performance vs. SNR for 2 sources at 1/2 nominal resolution as a function of the angular over-sampling M/N for $L=15$, $N=10$, and $\alpha=1/8$

Finally, we consider the impact of the parameter α used to scale the noise covariance term. Specifically, values of $\alpha=1$, $1/2$, $1/4$, $1/8$, and $1/16$ are examined for $M/N=16$,

$L = 15$ snapshots, and $N = 10$ antenna elements. Figures 7 and 8 depict the source separation and model order estimation performance, respectively. It is observed in Fig. 7 that for $N = 10$ antenna elements a value of $\alpha = 1/8$ appears to be the smallest acceptable value as the separation probability curve (top panel) for $\alpha = 1/16$ exhibits distinctively non-monotonically increasing behavior. It may be inferred that when α is too small the regularization provided by the noise covariance term becomes insufficient, especially at low values of SNR. It is also noted that reducing α by a factor of 2 (to within a limit as just observed) enables improved sensitivity by roughly a factor of 3 dB. A small decrease in RMS error is likewise found for smaller values of α , though the improvement is relatively minor.

In Fig. 8, model order estimation performance is illustrated as a function of α . Most notable is the fact that the $\alpha = 1/16$ implementation of RISR yields a significant over-estimation of model order between 0 and 20 dB SNR that coincides with the dip in performance observed for separation probability. Given that the separation probability metric requires that exactly two sources be detected within the allotted interval around $\psi = 0^\circ$ (via peaks in the RISR spectrum $\bar{\mathbf{x}}$) for the two true sources to be deemed separated, it may be deduced from the curves of $\alpha = 1/16$ that the low value of the scaled noise covariance term in this case is inducing spurious peaks to occur in the vicinity of the two closely-spaced sources. Hence, some lower bound on α is needed to prevent this effect from occurring.

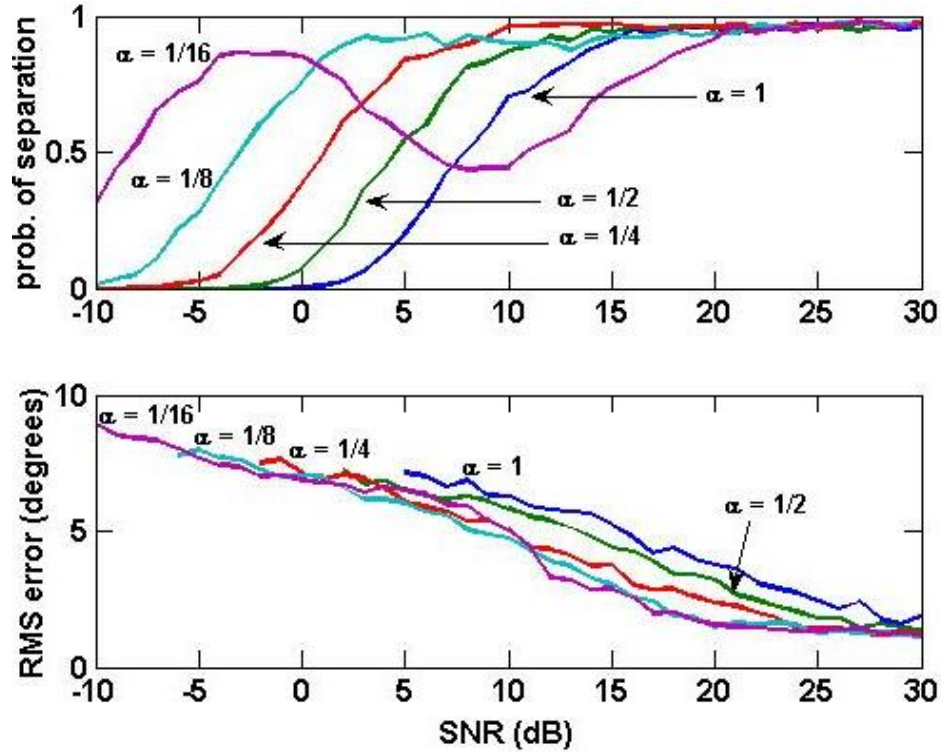


Figure 7. RISR: source separation performance vs. SNR for 2 sources (separation of 1/2 the nominal resolution) for various values of α with $L=15$, $M/N=16$, and $N=10$

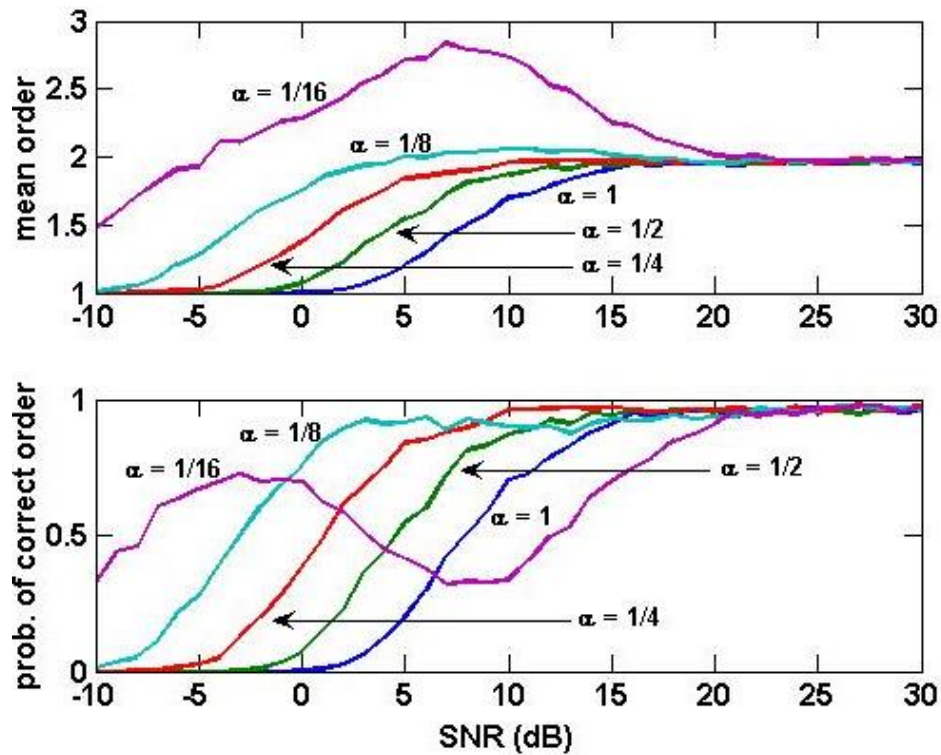


Figure 8. RISR: model order selection vs. SNR for 2 sources (separation of 1/2 the nominal resolution) for various values of α with $L=15$, $M/N=16$, and $N=10$

B. PERFORMANCE COMPARISON

We now compare RISR with the MUSIC, root-MUSIC (denoted RMUSIC here), and ESPRIT algorithms for various operating conditions. Super-resolution techniques employing the sample covariance matrix (SCM) generally perform well when the number of snapshots is high relative to the number of antenna elements (typically $L \geq 10N$ [4, pp. 947]). In contrast, RISR was shown to provide good performance for low sample support (see Figs. 2 and 3). In particular, as was shown in Fig. 3, RISR is capable of resolving K sources even when the number of snapshots $L < K$.

Here we shall consider the low sample support regime. For an array length of $N = 10$ elements we compare performance when $L = 15$ snapshots are available. We first assess the impact of modeling errors for 2 uncorrelated sources as a function of the degree of random gain/phase modeling error. We then consider the case of 4 sources present (with two closely-spaced in the vicinity of $\psi = 0^\circ$) with 1% gain/phase array modeling errors. The estimation of the 4 sources is first examined when they are uncorrelated and then when they are coherent (such as would occur in a multipath scenario). For the case involving coherent sources, the spatially-smoothed versions of MUSIC, RMUSIC, and ESPRIT employ a subarray size of $N_{ss} = 8$ thereby yielding $N - N_{ss} + 1 = 3$ subarrays. The 4-source scenarios (uncorrelated and coherent) are then re-examined when 5% array modeling errors are present.

For the source separation analysis of MUSIC, RMUSIC, and ESPRIT we assume that each algorithm possesses clairvoyant knowledge of the number of sources K . For these results RISR is implemented with noise covariance scaling $\alpha = 1/8$ and $M/N = 16$, and the array modeling error tolerance is known. Random amplitude and phase errors are assigned to each

antenna element independently for each Monte Carlo run. Per the generic model error defined in (18), for the Monte Carlo simulations here the n^{th} element is randomly generated as

$$z_n = \left[1 + \frac{\rho}{100} \mathcal{N}(0,1) \right] \exp \left\{ j\pi \frac{\rho}{100} \mathcal{N}(0,1) \right\} \quad (25)$$

with $\mathcal{N}(0,1)$ a Gaussian-distributed scalar with zero mean and unit variance and $\rho/100$ the percent error in terms of the standard deviation. For simplicity, the same percent error is assumed for both gain and phase. Given ρ , the error variance σ_z^2 is computed for RISR by estimating the variance of $z_m - 1$ from (25) for 1000 independent realizations.

Figures 9 and 10 illustrate the source separation and model order estimation performance, respectively, for two sources with 20 dB SNR separated by $1/2(\Delta\theta)_{\text{nom}} = 18^\circ$ with $L=15$ snapshots. In Fig. 9 the separation probability is depicted as a function of model error percentage. For low model error MUSIC, RMUSIC, and ESPRIT are found to be superior to RISR. However, as error increases it is observed that RISR experiences much more graceful degradation. Applying the MDL metric for model order estimation to the sample covariance matrix (SCM) and the spatially-smoothed SCM (denoted as MDL-SS) as a function of the model error percentage produces the curves in Fig. 10. It is observed that the model order estimate for RISR is much more robust to errors than MDL or MDL-SS, both of which tend to over-estimate the model order as the model error increases.

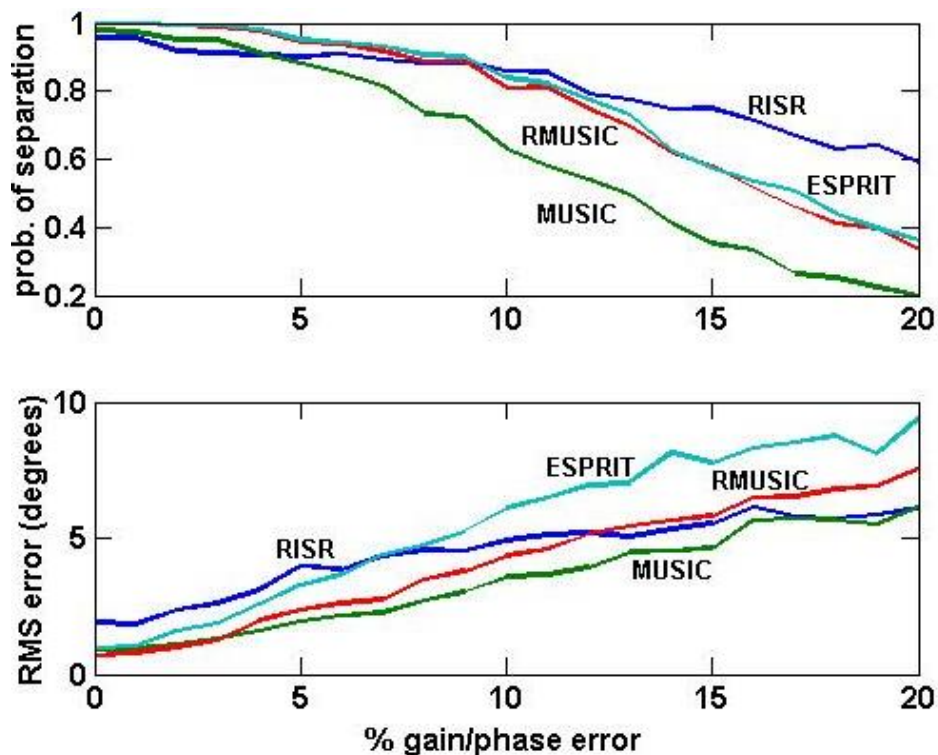


Figure 9. Source separation performance vs. percent gain/phase array errors for 2 uncorrelated sources (separated by $1/2$ the nominal resolution) with 20 dB SNR and $L = 15$ time samples

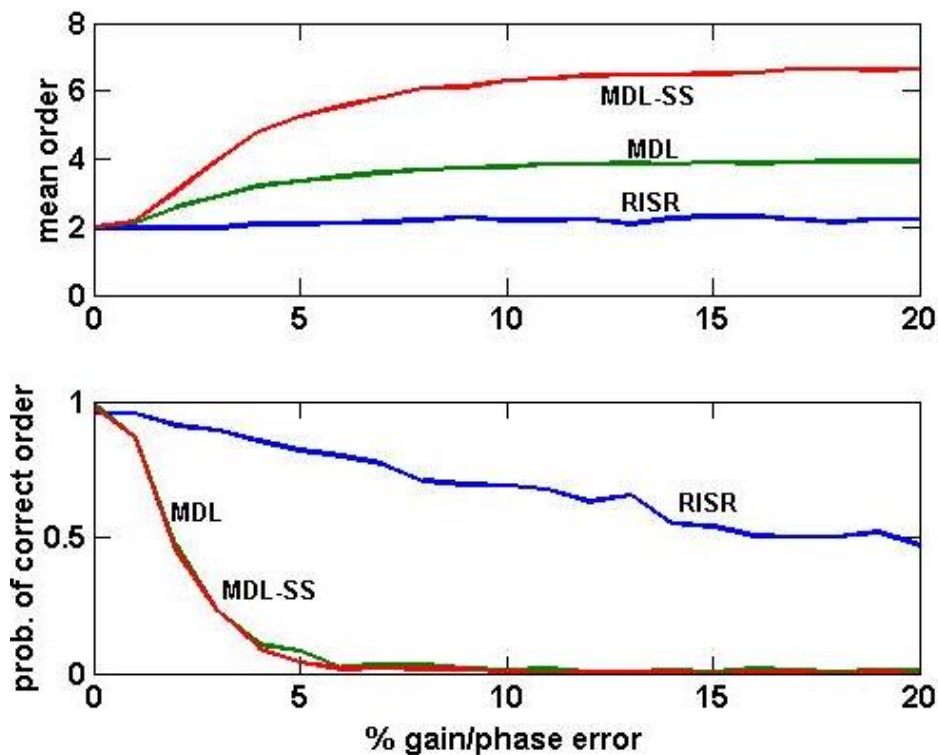


Figure 10. Model order selection vs. percent gain/phase array errors for 2 uncorrelated sources (separated by $1/2$ the nominal resolution) with 20 dB SNR and $L = 15$ time samples

For the case of 4 uncorrelated sources, two of which have $1/2(\Delta\theta)_{\text{nom}} = 18^\circ$ separation, Figs. 11 and 12 depict the source separation and model order estimation performance, respectively, for 1% random gain/phase errors ($\sigma_z^2 = -27$ dB for RISR).

In Fig. 11 it is observed that, in terms of probability of separation (top panel), RMUSIC, ESPRIT, and RISR provide similar performance. MUSIC, on the other hand, requires roughly 8 to 10 dB higher SNR to achieve the same level of performance as the other three algorithms. However, for RMS error (bottom panel) RISR is found to provide the least accuracy of the four techniques. With regard to model order estimation performance, it is observed in Fig. 12 that MDL and MDL-SS converge to the true model order of 4 from below while RISR slightly overestimates the model order (on average) at lower SNR and converges from above. However, as SNR increases above 15 dB the MDL and MDL-SS model order estimates are found to diverge as a result of the 1% random gain/phase errors array errors while RISR maintains the same estimate of 4 sources.

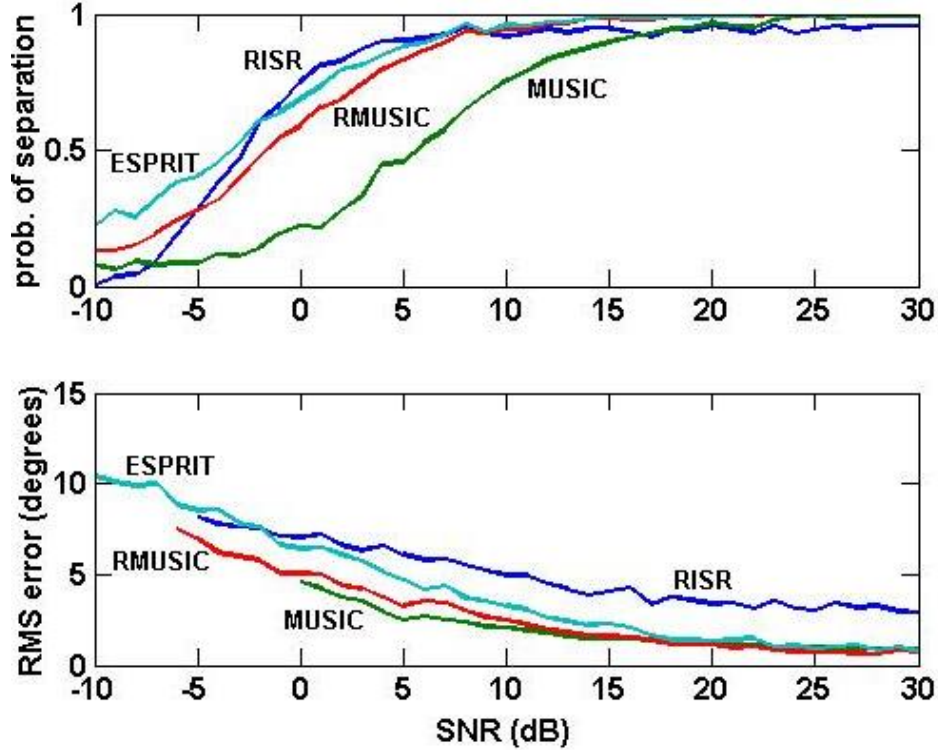


Figure 11. Source separation performance vs. SNR for 4 uncorrelated sources (2 with separation $1/2$ the nominal resolution), $L=15$ time samples, and 1% array modeling errors

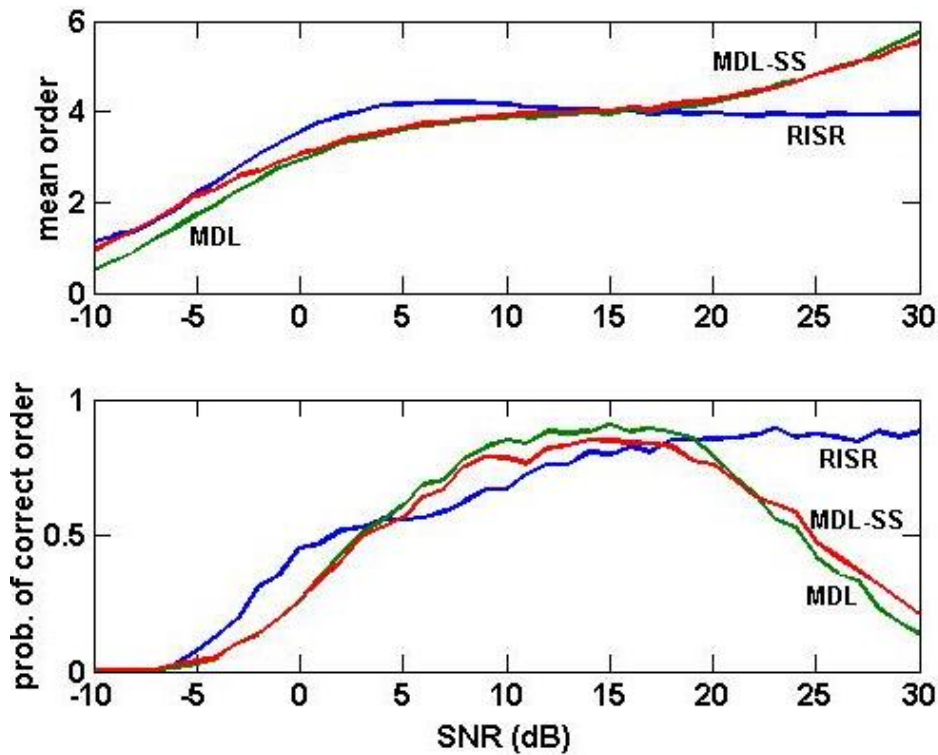


Figure 12. Model order selection vs. SNR for 4 uncorrelated sources (2 with separation $1/2$ the nominal resolution), $L=15$ time samples, and 1% array modeling errors

For the same scenario with 4 sources and 1% gain/phase errors, Figs. 13 and 14 depict the source separation and model order estimation performance when the 4 sources are coherent. In other words the same temporal signal arrives from different spatial angles albeit with different fading (gain and phase) characteristics. The fading is constant over the interval of L snapshots. Here the SCM-based techniques employ spatial smoothing.

In Fig. 13 we see that the performance comparison for separation probability is similar to what was observed in Fig. 11, although RISR now shows greater separation probability improvement at low SNR and levels off at approximately 75% (compared with ~90% for SS-RMUSIC and SS-ESPRIT and ~70% for SS-MUSIC). The RMS error has increased for all four algorithms relative to the uncorrelated case in Fig. 11, though the comparative relation between algorithms remains essentially the same with RISR yielding the highest error. In Fig. 14 it is observed that the MDL estimate (applied to the original SCM) is limited to 2 sources due to the rank deficiency of the SCM that results from source coherency. On the other hand the MDL-SS and RISR model order estimates remain quite similar to the uncorrelated case in Fig. 12 (top panel) with the primary difference being the lower probability of correct order (bottom panel).

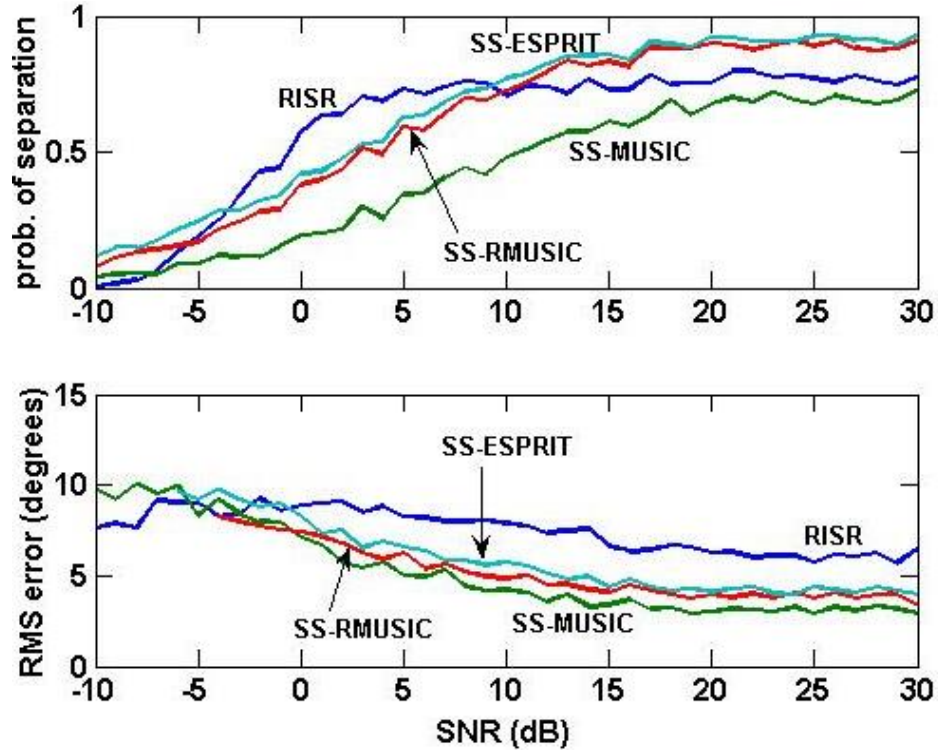


Figure 13. Source separation performance vs. SNR for 4 coherent sources (2 with separation 1/2 the nominal resolution), $L = 15$ time samples, and 1% array modeling errors

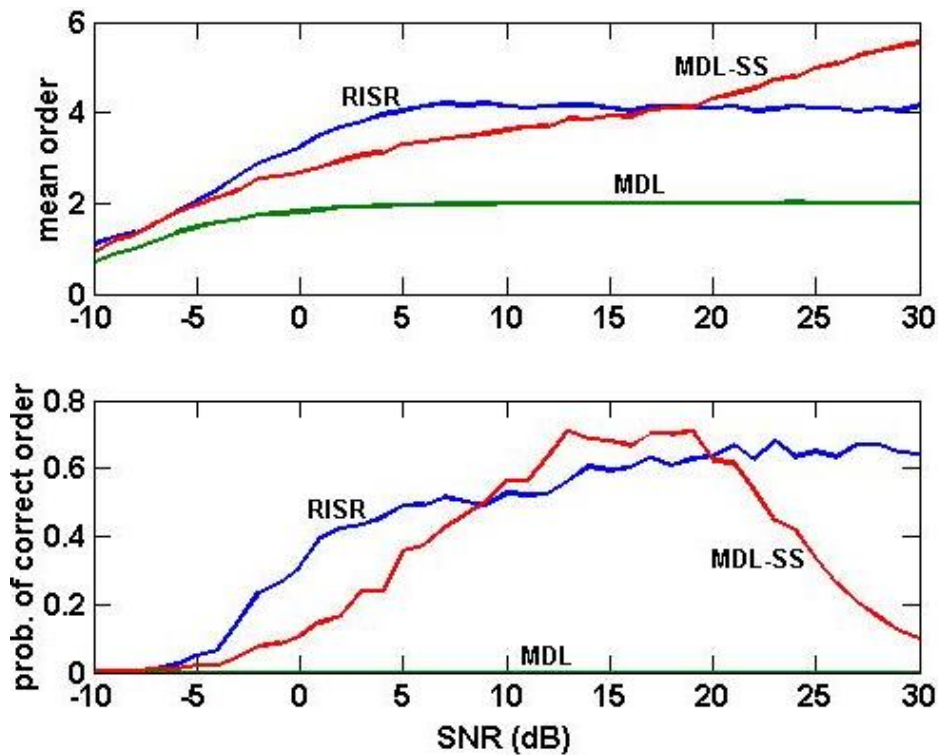


Figure 14. Model order selection vs. SNR for 4 coherent sources (2 with separation 1/2 the nominal resolution), $L = 15$ time samples, and 1% array modeling errors

Finally, we consider the performance of uncorrelated and coherent sources when the array model errors increase to 5% ($\sigma_z^2 = -16$ dB for RISR). Figures 15 and 16 contain the source separation and model order estimate performance for four uncorrelated sources. In Fig. 15 the separation probability (top panel) for all four methods is found to degrade a bit more relative to Fig. 11 as a result of the increase in model error. Again RISR performs close to RMUSIC and ESPRIT with all three being noticeably better than the MUSIC algorithm. Also, while RISR still provides the highest RMS error (bottom panel) of the four methods, the performance gap is now smaller. With regard to model error as shown in Fig. 16, the MDL and MDL-SS estimates are now significantly degraded, especially at high SNR, while the model order estimate of RISR is degraded a relatively small amount in comparison with the lower error result depicted in Fig. 12.

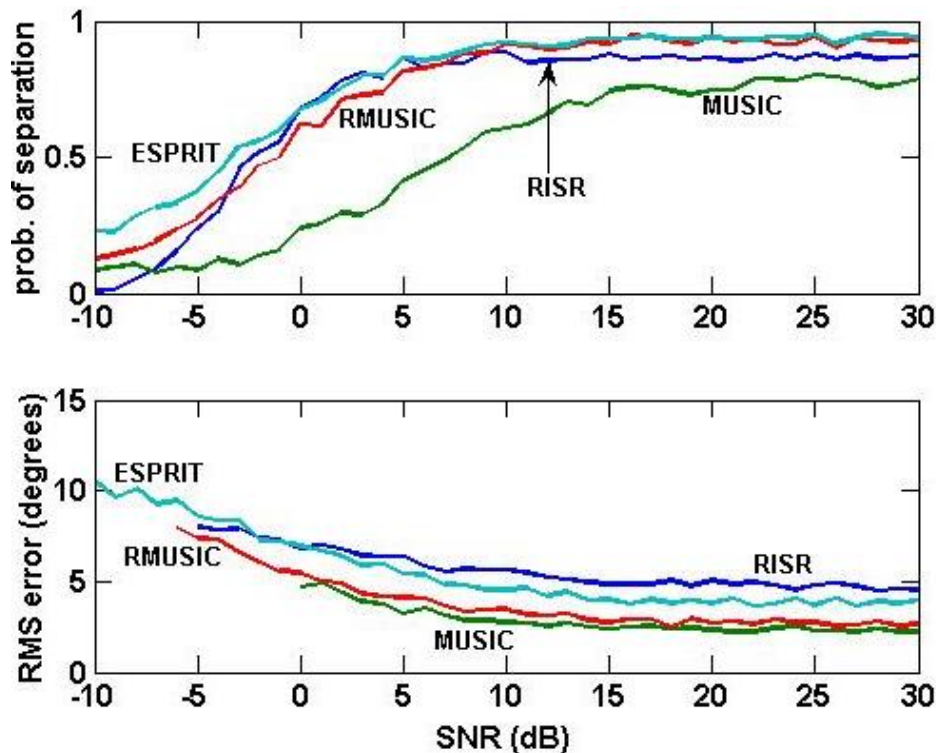


Figure 15. Source separation performance vs. SNR for 4 uncorrelated sources (2 with separation $1/2$ the nominal resolution), $L = 15$ time samples, and 5% array modeling errors

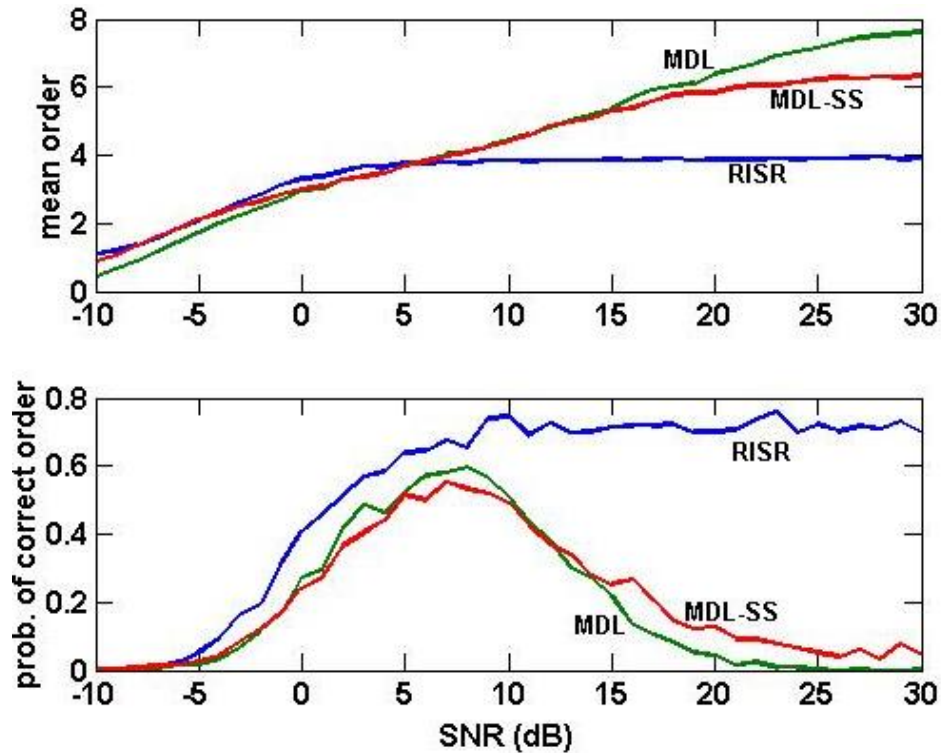


Figure 16. Model order selection vs. SNR for 4 uncorrelated sources (2 with separation 1/2 the nominal resolution), $L = 15$ time samples, and 5% array modeling errors

For four coherent sources with an array modeling error of 5%, Figs. 17 and 18 illustrate the source separation and model order estimate performance, respectively. In Fig. 17 it is found that RISR is now superior to the other three algorithms in terms of source separation performance (top panel). Also, the RMS error (bottom panel) is roughly commensurate for the four methods. Compared to the coherent source performance with lower modeling error from Fig. 14, it is observed in Fig. 18 that further degradation now occurs, though RISR is still markedly superior to either of the MDL estimates.

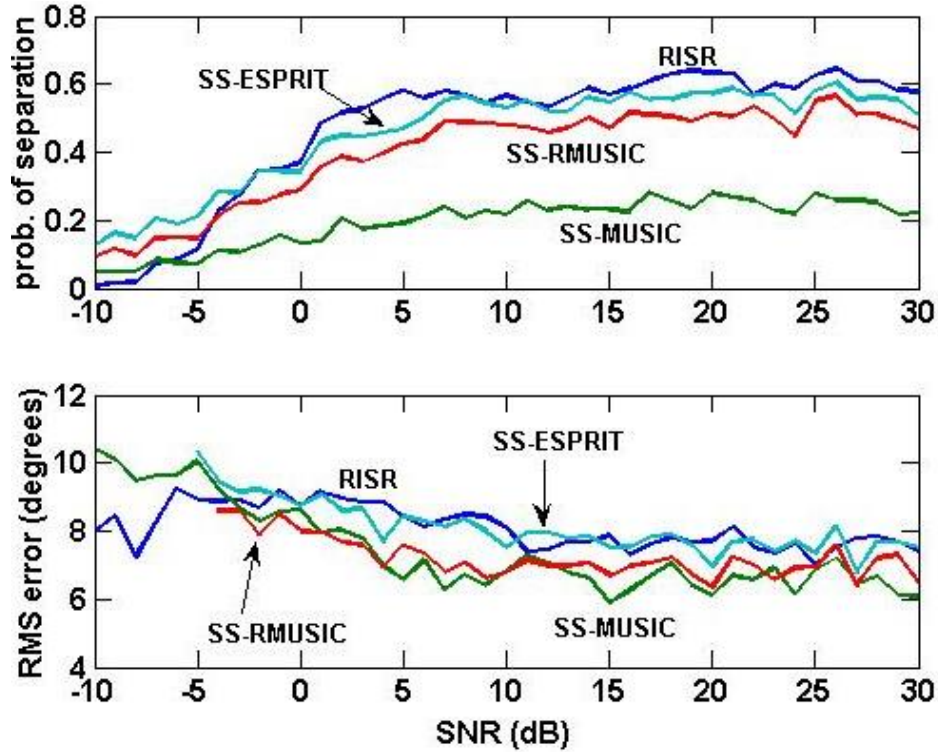


Figure 17. Source separation performance vs. SNR for 4 coherent sources (2 with separation 1/2 the nominal resolution), $L = 15$ time samples, and 5% array modeling errors

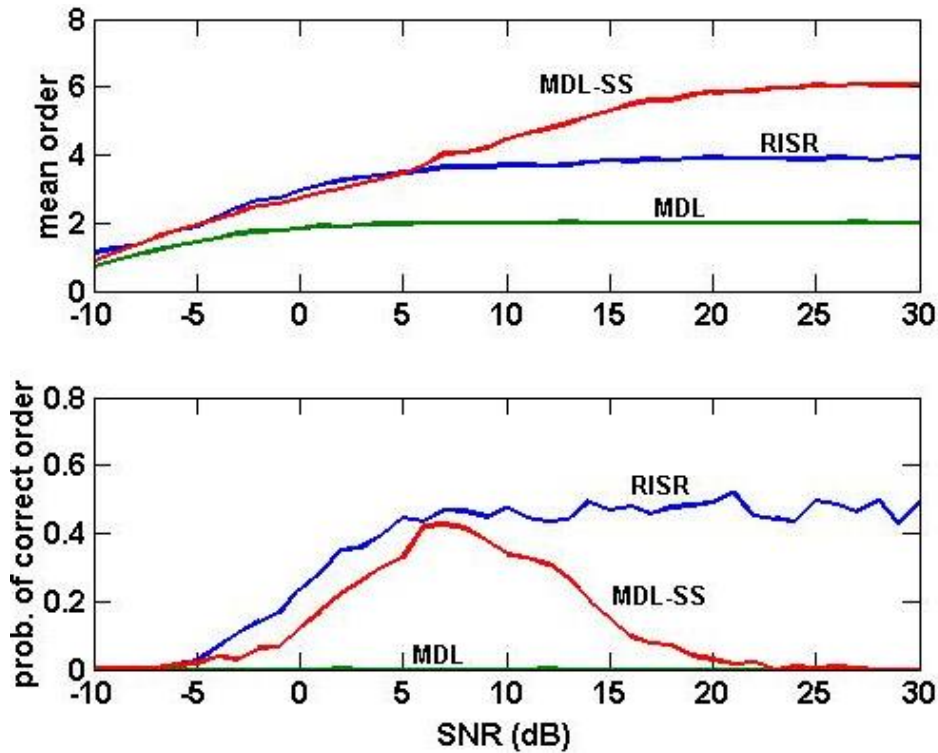


Figure 18. Model order selection vs. SNR for 4 coherent sources (2 with separation 1/2 the nominal resolution), $L = 15$ time samples, and 5% array modeling errors

CONCLUSIONS

A new method for direction-of-arrival (DOA) estimation is presented denoted as Re-Iterative Super-Resolution (RISR) that, like MUSIC, is applicable to arbitrary array structures as long as the array manifold is known. However, unlike methods such as MUSIC and ESPRIT which are based on the eigen-decomposition of a spatial covariance matrix (SCM), RISR is based on a minimum mean-square error (MMSE) formulation that is applied recursively and does not employ the SCM. RISR naturally estimates the number of sources, their locations (in ψ -space), and their power incident on the array, regardless of the temporal correlation of the sources. Additionally, RISR incorporates a non-coherent integration mechanism that enables significant gain in both probability of separation and angular RMS error. It is found that the additional performance gain afforded by non-coherent integration decreases as the number of samples increases and appears to approach an asymptotic bound after a relatively low number of samples. Finally, a structure for model error compensation has been developed and incorporated into RISR to account for unknown gain and phase errors that are present on all array elements in practice. This error compensation additionally provides an adaptive regularization term that facilitates greater sensitivity by making RISR robust to a reduction of the noise covariance term (which would otherwise produce line splitting and spurious peaks at high SNR).

For the linear array structure, simulation comparison demonstrates that for sample support on the order of the number of antenna elements, RISR yields separation probability commensurate with root-MUSIC and ESPRIT (which are not applicable to arbitrary array structures), though RISR possesses higher angle estimation error. As array modeling errors increase it is found that RISR degrades gracefully in terms of separation probability and remains quite robust for model order estimation.

REFERENCES

- [1] W.F. Gabriel, "Spectral analysis and adaptive array superresolution techniques," *Proceedings of the IEEE*, vol. 68, no. 6, pp. 654-666, June 1980.
- [2] W.F. Gabriel, "Adaptive processing array systems," *Proceedings of the IEEE*, vol. 80, no. 1, pp. 152-162, Jan. 1992.
- [3] H. Krim and M. Viberg, "Two decades of array signal processing research," *IEEE Signal Processing Magazine*, vol. 49, pp. 67-94, Apr. 1996.
- [4] H.L. Van Trees, *Optimum Array Processing*, John Wiley & Sons, Inc., New York, NY, 2002.
- [5] R.O. Schmidt, "Multiple emitter location and signal parameter estimation," *IEEE Trans. Antennas and Propagation*, vol. AP-34, pp. 276-280, Mar. 1986.
- [6] P. Stoica and A. Nehorai, "MUSIC, maximum likelihood, and the Cramer-Rao bound," *IEEE Trans. Acoustics, Speech, and Signal Processing*, vol. 37, no. 5, pp. 720-741, May 1989.
- [7] A. Paulraj, R. Roy, and T. Kailath, "A subspace rotation approach to signal parameter estimation," *Proceedings of the IEEE*, vol. 74, no. 7, pp. 1044-1046, July 1986.
- [8] J.E. Evans, J.R. Johnson, and D. F. Sun, "Application of advanced signal processing techniques to angle of arrival estimation in ATC navigation and surveillance systems," *MIT Lincoln Laboratory Technical Report*, June 1982.
- [9] A.J. Barabel, "Improving the resolution performance of eigenstructure-based direction-finding algorithms," *IEEE Intl. Conf. on Acoustics, Speech, and Signal Processing*, pp. 336-339, Apr. 1983.
- [10] N.J. Willis, *Bistatic Radar*, SciTech Publishing Inc., Raleigh, NC, 2005.
- [11] J.E. Evans, J.R. Johnson, and D.F. Sun, "High resolution angular spectrum estimation techniques for terrain scattering analysis and angle of arrival estimation," *Proc. 1st ASSP Workshop on Spectral Estimation*, pp. 134-139, 1981.
- [12] T. Shan, M. Wax, and T. Kailath, "On spatrial smoothing for direction-of-arrival estimation of coherent signals," *IEEE Trans. Acoustics, Speech, and Signal Processing*, vol. ASSP-33, No. 4, pp. 806-811, Aug. 1985.
- [13] A.L. Swindlehurst and T. Kailath, "Performance analysis of subspace-based methods in the presence of model errors, part I: the MUSIC algorithm," *IEEE Trans. Signal Processing*, vol. 40, no. 7, pp. 1758-1774, July 1992.
- [14] A.J. Weiss and B. Friedlander, "Effects of modeling errors on the resolution threshold of the MUSIC algorithm," *IEEE Trans. Signal Processing*, vol. 42, no. 6, pp. 1519-1526, June 1994.
- [15] M. Jansson, A.L. Swindlehurst, and B. Ottersten, "Weighted subspace fitting for general array error models," *IEEE Trans. Signal Processing*, vol. 46, no. 9, pp. 2484-2498, Sept. 1998.

- [16] A. Ferreol, P. Larzabal, and M. Viberg, "On the resolution probability of MUSIC in presence of modeling errors," *IEEE Trans. Signal Processing*, vol. 56, no. 5, pp. 1945-1953, May 2008.
- [17] C. Roos, T. Terlaky, and J.-P. Vial, *Interior Point Methods for Linear Optimization*, Springer, New York, NY, 2006.
- [18] S.A. Ruzinsky and E.T. Olsen, " L_1 and L_∞ minimization via a variant of Karmarkar's algorithm," *IEEE Trans. Acoustics, Speech, and Signal Processing*, vol. 37, no. 2, pp. 245-253, Feb. 1989.
- [19] I. F. Gorodnitsky and B. D. Rao, "Sparse signal reconstruction from limited data using FOCUSS: a re-weighted minimum norm algorithm," *IEEE Transactions on Signal Processing*, vol. 45, No. 3, pp. 600-616, Mar. 1997.
- [20] I. Dotlic and A. Zejak, "Pattern sidelobe level suppression on antenna array with arbitrary geometry by the IRLS algorithm," *International Conference on Trends in Communications*, pp. 167-177, July 4-7, 2001.
- [21] J. Li and P. Stoica, *Robust Adaptive Beamforming*, John Wiley & Sons, Inc., Hoboken, NJ, 2006, Chap. 5.
- [22] Y.I. Abramovich, N.K. Spencer, and A.Y. Gorokhov, "Resolving manifold ambiguities in direction-of-arrival estimation for nonuniform linear antenna arrays," *IEEE Transactions on Signal Processing*, vol. 47, no. 10, pp. 2629-2643, Oct. 1999.
- [23] J. T.-H. Lo and S.L. Marple Jr, "Observability conditions for multiple signal direction finding and array sensor localization," *IEEE Transactions on Signal Processing*, vol. 40, no. 11, pp. 2641-2650, Nov. 1992.
- [24] S.D. Blunt and K. Gerlach, "Adaptive pulse compression via MMSE estimation," *IEEE Trans. Aerospace and Electronic Systems*, vol. 42, no. 2, pp. 572-584, Apr. 2006.
- [25] S.D. Blunt, T. Chan, and K. Gerlach, "A New Framework for Direction-of-Arrival Estimation," *5th IEEE Sensor Array and Multichannel Processing Workshop*, Darmstadt, Germany, July 21-23, 2008.
- [26] J. Rissanen, "Modeling by shortest data description," *Automatica*, vol. 14, pp. 465-471, 1978.
- [27] P. Chen, T.-J. Wu, and J. Yang, "A comparative study of model selection criteria for the number of signals," *IET Radar, Sonar, & Navigation*, vol. 2, no. 3, pp. 180-188, June 2008.